# Differences in cloud microphysical properties between MODIS Collections 5.1 and 6

John Rausch[1], Kerry Meyer[2,3], Ralf Bennartz[1,4] and Steven Platnick[3]

[1]Department of Earth and Environmental Sciences, Vanderbilt University, Nashville, TN 37235, USA
5   [2]Goddard Earth Science Technology and Research, Universities Space Research Association, Columbia, MD 21046, USA
[3]NASA Goddard Space Flight Center, Greenbelt, Maryland, 20771, USA
[4] Space Science and Engineering Center, University of Wisconsin – Madison, Madison, WI 53706, USA

*Correspondence to*: John Rausch (john.rausch@vanderbilt.edu)

**Abstract.** Differences in cloud effective radius and cloud droplet number concentration (CDNC) estimates inferred from the Aqua MODIS Collections 5.1 and 6 cloud products (MYD06) are examined for warm clouds over global oceans for the year 2008. Individual pixel level retrievals for both collections are aggregated to 15   1° x 1° and compared globally and regionally for the three main spectral channel pairs used for MODIS cloud optical property retrievals. Comparisons between both collections are performed for cases in which all channel pairs are successfully retrieved for each pixel and for cases where one or more channel pairs are successful. The contribution to the observed differences of several key MYD06 Collection 6 algorithm updates are also explored. Global results show a neutral to positive (> 50 cm$^{-3}$) change for C6-derived CDNC relative to C5.1 for the 1.6 and 2.1 μm channel retrievals corresponding to 20   a neutral to -2 μm difference in droplet effective radius. For 3.7 μm retrievals, CDNC results show a negative change in the tropics, with differences transitioning towards positive values with increasing latitude spanning (-25 to +50 cm$^{-3}$) related to a (+2.5 to -1 μm) transition in effective radius. Regionally, the magnitude and behavior of the annual CDNC cycle are compared for each retrieval channel pair. Results from this study indicate significant intercollection differences in aggregated values of microphysical parameters which may have implications for existing MODIS derived climatologies and 25   validation studies.

## 1 Introduction

Marine stratocumuli play a large role in the modulation of the Earth's radiative balance and hydrological cycle, owing to their persistence and large areal extent. They are maintained by moisture flux from the sea surface, longwave

cooling and dry air entrainment at the cloud top. Confined to the planetary boundary layer, most often in subtropical subsidence areas, they are susceptible to the influences of anthropogenic aerosols. Aerosol perturbation manifests changes though several mechanisms: Through the first indirect aerosol effect, anthropogenic influences potentially alter the degree of rejection of shortwave radiation by distributing a given quantity of cloud water over a larger number of droplets compared

5    to an unperturbed cloud by supplying additional cloud condensation nuclei (CCN) (Twomey, 1974). This increase in cloud albedo provides a local cooling effect as the cloud top temperature is near the sea surface temperature, producing a negligible longwave radiative forcing. With a decrease in droplet effective radius from the addition of CCN, autoconversion efficiency can decrease reducing precipitation efficiency (Albrecht, 1989) and also potentially the overall lifetime of clouds, augmenting the $1^{st}$ indirect effect (Lohmann and Feichter, 2005). This naturally leads to a need for estimates of cloud

10   droplet concentration from observation to better understand the natural background and anthropogenic contributions to cloud droplet number concentration.

Satellites offer an opportunity to address this need through their global observational area spanning decades. The National Aeronautics and Space Administration's (NASA) Moderate Resolution Imaging Spectroradiometer (MODIS) is an instrument suited for this task. Flown aboard two Earth observing satellites (Terra and Aqua), MODIS provides

15   observations in the appropriate spectral bands to infer cloud optical thickness and droplet effective radius through the bi-spectral method of Nakajima and King (1990). From the retrieved properties of cloud optical thickness and droplet effective radius, cloud droplet number concentration can be estimated (Brenguier et al., 2000). NASA provides retrievals of the cloud optical properties through the MODIS Cloud Product (MOD06 and MYD06 for Terra and Aqua, respectively; note the MOD06 and MYD06 algorithms are nearly identical (Platnick et al., 2015), (Platnick et al., in revision, 2016). As passive

20   imager cloud remote sensing science evolves, the MODIS Cloud Product undergoes periodic updates to the cloud screening and retrieval algorithms that are collectively implemented and reprocessed as "collections." Collection 6 is the most recent release of the Cloud Product and includes several changes that propagate through to estimates of cloud microphysical properties relative to its predecessor, Collection 5.1 (Platnick et al., 2015). As there is a considerable body of research based upon Collection 5.1 of effective radius e.g. (Zhang and Platnick, 2011), (Painemal and Zuidema, 2011) and CDNC e.g.

25   (Zeng et al., 2014), (Ahmad et al., 2013) there is a need to understand how these retrievals differ between collections, which

may help explain differences in the investigations performed with their data. In this study we investigate and highlight the differences in cloud microphysical estimates manifested both in effective radius and CDNC between both collections using one year of Aqua MODIS (MYD06) observations of warm clouds over global oceans in an attempt to understand the differences in CDNC from the respective products.

5 **2 Data and Methods**

The MODIS Collection 5.1 (C5.1) Cloud Product provides estimates of cloud optical thickness ($\tau$) and droplet effective radius ($r_e$) in addition to cloud screening, quality control flags and ancillary data relevant to the computation of cloud droplet number concentration. For most parameters derived from visible and near/shortwave infrared channels, the spatial resolution is 1 x 1 km at nadir. Some parameters, such as those derived from thermal infrared channels, are provided

10 at a 5 x 5 km resolution. The C5.1 Cloud Product applies a Clear Sky Restoral (CSR) algorithm that identifies pixels that are expected to be only partially cloudy and excludes them from the cloud optical properties retrieval, essentially limiting C5.1 data to overcast scenes only. In addition, the C5.1 $r_e$ retrievals using the 1.6 and 3.7 μm channels are given as a difference relative to the 2.1 μm $r_e$ value, and are therefore dependent upon the success of the 2.1 μm retrieval.

The Collection 6 (C6) Cloud Product offers improvements in retrievals of several relevant parameters for CDNC

15 estimation. Changes to the optical and microphysical retrievals for C6 include improvements to the forward radiative transfer model used to create the pre-calculated cloud retrieval look-up tables, re-registration of the visible/near IR focal planes for MODIS Aqua, and explicit reporting of all three spectral channel pair effective radius retrievals (Platnick et al., 2015); cloud top property retrieval changes for C6 include additional cloud top temperature and pressure retrievals at 1 x 1 km spatial resolution and improvements to the characterization of low-level clouds over water surfaces, among others

20 (Menzel et al., 2008), (Baum et al., 2012). With respect to the assessment of pixel quality, the CSR algorithm is still applied and its results reported in the cloud product, but unlike C5.1, cloud optical property retrievals are attempted on pixels identified as partly cloudy and, if successful, are written to the cloud product separate from the heritage overcast retrievals (Platnick et al., 2015); note that pixels identified by the CSR algorithm as being not cloudy (e.g., false cloudy sun glint or thick aerosols such as smoke or dust) remain excluded from the cloud optical property retrievals. One year of MODIS Aqua

25 C5.1 and C6 data, corresponding to calendar year 2008, is used in this investigation.

### 2.1 Calculating CDNC

Relating cloud droplet number concentration to retrievals of optical thickness and droplet effective radius requires an estimate of cloud liquid water content. To attain that quantity, the vertical structure is assumed to follow the so-called adiabatically-stratified cloud model (Brenguier et al., 2000). This model accounts for a linear increase in cloud liquid water

5  content as a saturated air parcel rises through a cloud's vertical extent while undergoing droplet growth as the parcel cools moist adiabatically. As marine boundary layer clouds are typically shallow, the temperature is nearly constant, so it follows that the amount of condensate formed through adiabatic ascent can be assumed to be constant. The adiabatic liquid water content $w_{AD}$ at any point $h$ above the cloud base can be expressed as:

$$w(h,T) = c_w(T)h \qquad (1)$$

where $c_w$ is the mass of condensate formed per unit volume for each meter of ascent and $T$ is the cloud top temperature. The $c_w$ parameter is derived from the Clausius-Clapeyron relationship, and is primarily a function of temperature and to a lesser degree, pressure. For this study, an assumed cloud top pressure of 850 hPa is used, which corresponds to a geopotential

15  height of approximately 1500 m. For marine stratocumulus regions such as the Southeast Pacific, this height is near the mean top of the boundary layer (von Engeln and Teixeira, 2013) around Aqua's 13:30 local equatorial crossing time (Ho et al., 2015).

Relating the liquid water content profile to the cloud optical properties Brenguier et al. (2000) express the adiabatic liquid water path as:

$$W_{AD} = \frac{5}{9}\rho_l \tau r_{e,top} , \qquad (2)$$

where the effective radius is the value at cloud top. Accounting for cloud top entrainment of dry air, observed and modeled liquid water paths are typically near 80% of the purely adiabatic value (Duynkerke et al., 2004), (Pawlowska and Brenguier,

2003). The $c_w$ parameter in this study is therefor scaled to approximately 80% of the purely adiabatic value, in order to avoid overestimation of the condensate observed by MODIS.

With the cloud optical parameters, Bennartz (2007) expresses CDNC as:

$$N = \frac{\tau}{k}[2W]^{-5/2}\left[\frac{3}{5}\pi Q\right]^{-3}\left[\frac{3}{4\pi\rho_l}\right]^{-2}c_w^{1/2} \qquad (3)$$

where $k$ encapsulates that skewness and dispersion of the cloud droplet size distribution, $Q$ is the scattering efficiency and $\rho_l$ is the density of liquid water. For marine boundary layer clouds $k=0.8$ is assumed to be a representative value for this study (Brenguier et al., 2011), (Martin et al., 1994), although Painemal and Zuidema (2011) suggest that $k=0.88$ may be more

10 representative for droplets near the cloud top, resulting in a narrower cloud droplet size distribution. As the size parameters for cloud droplets approach the geometric optics limit, the asymptotic value of 2 is assumed for $Q$.

### 3 Results

#### 3.1 Global-Scale Common Pixel Comparison

Common pixel scenes are those in which valid retrievals exist for all three effective radii retrievals, independent of

15 vertical stratification, for both collections with otherwise consistent selection criteria. The primary advantage of this is a 1:1 pixel-level comparison between both collections, allowing for an objective comparison of effective radius and CDNC free of the influence of pixel population differences due to, e.g., changes to the cloud thermodynamic phase algorithm between collections (Marchant et al., 2016) or spectrally-dependent retrieval failure rate patterns (Cho et al., 2015). The global distribution of the total MODIS Aqua common pixel count for calendar year 2008 is shown in Fig. 1.

20 Mean annual differences in MYD06 cloud droplet effective radius, aggregated globally to a 1° x 1° equal angle grid for calendar year 2008, from the 1.6, 2.1 and 3.7 μm channels are shown in Fig. 2a-c. For the $r_{e,1.6}$, C6 retrievals are smaller than C5.1 over most of the global oceans (differences generally less than -1 μm), with the largest differences (greater than -2 μm) occurring near the Baja California peninsula. In equatorial regions of the Indian and West Pacific Basins, as well as over sea ice regions in the northern high latitudes above 60° N, however, $r_{e,1.6}$ differences are largely neutral to slightly

positive. C6 retrievals of $r_{e,2.1}$ are predominantly smaller than C5.1 (differences less than -1 μm) with the greatest

disagreement between collections occurring in the tropics. For $r_{e,3.7}$ there is a latitudinal gradient in the retrieval differences,

with positive intercollection differences in the topics (C6 > C5.1 by more than 2 μm) transitioning to slightly negative values

(C6 < C5.1 by less than -2 μm) at higher latitudes.

5    Patterns similar to those found in the effective radius differences are mirrored in the respective CDNC difference

plots. As shown in Fig. 3a-b., for the $N_{1.6}$ and $N_{2.1}$ estimates, the differences are generally neutral to positive, i.e., C6 > C5.1,

with values over +50 cm$^{-3}$ occurring along coastal boundaries in the subtropical subsidence zones. Fig. 3c shows the

differences in $N_{3.7}$ are significantly different, with C6 CDNC smaller than C5.1 in the tropics and generally larger at latitudes

higher that 45°. Note that of the three spectral channels used for $r_e$ retrievals, the sensitivity of the 3.7μm channel is weighted

10   closest to cloud top (Platnick, 2000), and $r_{e,3.7}$ is therefore considered to be the most appropriate effective radius for

estimating CDNC based upon the assumptions of the adiabatic model.

### 3.2 Algorithmic and calibration factors in intercollection differences

Due to the strong sensitivity to effective radius ( $N \propto r_e^{-5/2}$ ) in Equation 3, larger effective radii translate into lower

15   relative CDNC (and vice versa), thus the $r_e$ differences shown in Fig. 2 largely explain the CDNC differences observed in

Fig. 3. As previously noted, the use of common pixels in the analysis in Section 3.1 removes the influence of pixel

population differences between the two collections. The large effective radius differences between C5.1 and C6 observed in

Fig. 2 are therefore the result of either changes to the MYD06 optical property retrieval algorithm itself or changes to

upstream or ancillary products such as the Level 1b calibrated radiometric data or the MYD06 cloud top property retrieval

20   algorithm.

For C6, changes to the liquid phase cloud optical property retrievals were, for the case of $r_{e,1.6}$ and $r_{e,2.1}$, limited

primarily to the pre-computed retrieval look-up tables (LUTs). The most significant of these LUT changes is the inclusion of

an ocean surface bidirectional reflectance model that uses the Cox-Munk wind speed and direction-dependent wave-slope

distribution (Cox and Munk, 1954a,b); previously in C5.1 the ocean surface was assumed to be a Lambertian reflector with

25   5% albedo. This change primarily impacts $r_e$ retrievals for optically thinner clouds (τ roughly < 2 to 3) and those over sun

glint, lowering $r_e$ by up to 1 μm. The strength of this effect is dependent on the orthogonality of the solution space, and thus

the impacts are largest for $r_{e,1.6}$ and smallest for $r_{e,3.7}$. These $r_e$ decreases due to LUT changes can be offset or enhanced,

depending on the location of the pixel relative to cloud illumination or shadowing, by the effects of the Aqua Level 1b re-

registration of the visible/near-IR focal plane, the effects of which are again strongest on $r_{e,1.6}$ due to enhanced LUT non-

5    orthogonality (note $r_{e,3.7}$ is largely unaffected). The largest contribution to the $r_e$ changes observed in Fig. 2, however, in

particular for $r_{e,1.6}$ and $r_{e,2.1}$, is that resulting from the updates to the cloud top pressure (CTP) retrievals. As shown in Fig. 4a,

C6 CTP is largely higher than in C5.1, with increases of 100 hPa or more over the marine stratocumulus regions, though in

regions where the liquid cloud occurrence is low (e.g., the tropics; see Fig. 1) C6 CTP slightly decreases. Higher CTP, i.e.,

lower cloud top height, results in larger above-cloud atmospheric gaseous absorption corrections, brighter top of cloud

10   reflectance, and thus smaller $r_e$ from all three spectral channels, by up to 1 μm or more.

While the above C6 changes largely explain the intercollection differences for $r_{e1.6}$ and $r_{e2.1}$, algorithm updates for

the $r_{e3.7}$ retrieval were more extensive, involving fixes to known shortcomings in the C5.1 algorithm, and their net

contribution to the dissimilar difference patterns shown in Fig. 2 are unclear. Retrieved $r_{e3.7}$ decreases resulting from the CTP

changes are enhanced by a correction to the assumed band-averaged solar irradiance ($F_0$) at 3.7μm. For C6, $F_0$ is smaller than

15   for C5.1 and earlier versions (10.9 Wm$^{-2}$μm$^{-1}$ for C6 versus 11.7 Wm$^{-2}$μm$^{-1}$ for C5.1), resulting in a decrease of $r_{e,3.7}$ by 1 μm

or more. However, above-cloud atmospheric emission, previously ignored in C5.1, is now accounted for in C6 and yields

sizably larger $r_{e,3.7}$, on the order of 1 μm or more. For a single granule case study off Baja California (not shown), the

cumulative effect of the C6 changes discussed here appear to explain the observed granule-level intercollection $r_{e,3.7}$

differences, which for the case study granule are strongly positive (C6 larger) or negative (C6 smaller) and are seemingly

20   dependent on view angle. Nevertheless, it is difficult to determine how the granule-level $r_{e,3.7}$ differences translate to the

global aggregated differences in Fig. 2, and given the extensive C6 changes and the known shortcomings of the C5.1 $r_{e,3.7}$

retrievals it is of limited benefit to further assess their intercollection differences.

Finally, an additional consideration regarding the intercollection CDNC differences shown in Fig. 3 is the fact that

CDNC estimates from the retrieved cloud optical properties also depend on the retrieved cloud-top temperature (CTT)

25   through the $c_w$ parameter. As discussed above and in Section 2, a number of algorithm improvements were implemented in

the C6 MYD06 cloud-top property product, including cloud-top retrievals at 1 km resolution in addition to the 5km cloud-top retrievals that have heritage to C5.1 and earlier collections (Baum et al., 2012). For the C6 CDNC estimates in this study, the 1 km CTT is used. To assess the impact of differences in CTT on CDNC, the CTT values from C5.1 at 5 km and C6 at 1 km were aggregated to 1° x 1° for the common pixel population, shown in Fig. 4b. The differences in CTT reveals a

5   relatively lower temperature (3K) from C6 in subsidence regions at low latitudes, neutral to slightly positive differences at higher latitudes and largely positive differences in the intertropical convergence zone (ITCZ). To determine how the disagreement in CTT translates to CDNC apart from the cloud-top retrieval impacts to $r_e$, the $c_w$ was also aggregated to 1° x 1°. The differences in $c_{w,6}$ and $c_{w,5.1}$ translate to a 0.5% relative decrease in globally averaged $N$ for C6, provided all other parameters are held constant. However, in the subtropical subsidence regions, the decrease is near 4%. Therefore, $c_w$ has

10   only a marginal impact on $N$ for any of the three absorption channels, a result that provides further evidence in favor of attributing intercollection $N$ differences largely to changes in the effective radius retrievals.

### 3.3 Independent Pixel Comparison

An additional improvement in C6 is the explicit reporting of all three effective radii retrievals. In prior collections, the 1.6 and 3.7 μm retrievals are given as a difference relative to the 2.1 μm $r_e$. Therefore, reporting $r_e$ for either of these

15   channels depends upon the success of the $r_{e,2.1}$ retrieval. Assessing the differences in the level 3 CDNC from C6 for cases where all three retrievals were valid for a given pixel (i.e., common pixel sampling) relative to cases where a given spectral retrieval was valid regardless of the success of the other two spectral retrievals (i.e., independent pixel sampling), Fig. 5 shows the estimate of $N_{1.6}$ using independent pixel sampling is about 10 cm$^{-3}$ higher globally relative to the common pixel population during September through March and as much as 40 cm$^{-3}$ between April and August. The independent $N_{2.1}$ value

20   slightly underestimates the common $N_{2.1}$ systematically by approximately 5 cm$^{-3}$ and, rather surprisingly, both $N_{3.7}$ retrievals are largely in agreement with each other.

Approximately ½ of the Aqua MODIS 1.6 μm 500 m detectors are non-functional, and four out of every ten 1 km pixel rows in each across track scanline contain no 1.6 μm reflectance observations and thus no $r_{e,1.6}$ retrievals. With the independent pixel selection criterion, pixels from the rows containing the non-functional 1.6 μm detectors are sampled for

25   the 2.1 and 3.7 μm channels and therefore dominate the population of additional pixels gained in each case. Because the

rows corresponding to non-functional 1.6 μm detectors are evenly distributed throughout each granule, no sampling bias is expected with respect to the rows having functional detectors, and the aggregated retrieval statistics of functioning and non-functioning detector rows are likely to be nearly identical. The better agreement between the common and independent populations for $N_{2.1}$ and $N_{3.7}$ is thus likely attributable to the inclusion of a large number of independent pixels having similar

5    $r_e$ statistics as the common pixel criteria. For $N_{1.6}$, on the other hand, the additional pixels gained are limited only to those cases where the $r_{e,2.1}$ or $r_{e,3.7}$ retrievals failed, making it inherently more sensitive and explaining, at least to some extent, the greater differences observed in $N_{1.6}$ under the independent pixel criterion.

### 3.4 Regional Common Pixel Comparison

Four maritime regions were selected for additional examination primarily for their proximity to sources of

10    anthropogenic aerosols and generally high number of cloud observations within their domains:  Southern Africa (SAF), South America (SAM), North America (NAM) and Southeast Asia (SEA).  The boundaries of these regions are shown as white outlines in Fig. 1.

The annual CDNC cycles from C5.1 and C6 are given in Fig. 6a for the Southern Africa region.  Similar to the global results, the 1.6 and 2.1 μm CDNC from C6 are systematically higher (>10 cm$^{-3}$), while the C6 3.7 μm values vary

15    from being lower (< 10 cm$^{-3}$) to near agreement with C5.1.  During the African dry biomass burning season between May and September (Roberts et al., 2009), the 1.6 μm C6 CDNC presents the greatest differences between collections exceeding 30 cm$^{-3}$ at this maximum CDNC over 180 cm$^{-3}$.  Interestingly, there is a discernable difference at 3.7 μm for both collections over the biomass season, however it is quite muted relative to $N_{1.6}$; peak values during the season are roughly in agreement with Austral summer values between 90-100 cm$^{-3}$.  Results from the SAM region in Fig. 6b show a stratification and general

20    response between collections which is similar to SAF.  Although, a generally consistent aerosol emission rate gives rise to little variability (Huneeus et al., 2006), with annual cycle amplitudes limited to a range of approximately 20 cm$^{-3}$ across all channels for both collections.  For NAM, the common pixel comparison also yields similar results as the previous regions as shown in Fig. 6c.  For this region, both the 1.6 and 2.1 μm channels also exhibit a 20 – 30 cm$^{-3}$ bias for collection 6 retrievals while 3.7 μm in near agreement with Collection 5.1.  All three channels have a uniform response to increases in CDNC

coincident with a relatively early wildfire season that occurred during the spring and summer of 2008 in California (Brioude et al., 2009).

In contrast to the other regions in the study, the SEA domain yields a different stratification of CDNC shown in Fig. 6d, where $N_{3.7} > N_{1.6} > N_{2.1}$ for both collections with general agreement between $N_{3.7}$ retrievals. Disagreements between

5    collections are less than 15 cm$^{-3}$ for each channel. The different stratification may be a result of differing cloud dynamics in a region due to a weaker inversion strength resulting in greater entrainment compared the other regions which lie in subsidence zones. There is a strong seasonal response to aerosols visible in each channel coincident with the advection of aerosols by the Asian winter monsoon (Bennartz et al., 2011).

### 4. Conclusions

It has previously been shown that, under the condition of adiabatic clouds, estimates of the CDNC of warm marine liquid phase clouds can be derived from passive satellite remote sensing observations. To this end, observations from MODIS on the Terra and Aqua satellites has seen wide use. The operational MODIS Cloud Product (MYD06 for Aqua) provides the cloud property retrievals necessary for computing CDNC estimates, namely cloud-top temperature, cloud

15   optical thickness, and effective droplet radius ($r_e$). Collection 6, the most recent release of MYD06, includes numerous updates relative to its predecessor, Collection 5.1, that can propagate through to estimates of CDNC. Using one year (2008) of global MODIS Aqua observations, intercollection differences are investigated for CDNC derived from three independent spectral re retrievals, namely from the 1.6, 2.1, and 3.7μm channels. For the pixel population having successful $r_e$ retrievals from all three spectral channels in both collections, C6 $r_{e,1.6}$ and $r_{e,2.1}$ retrievals are smaller than those of C5.1, with the

20   greatest differences generally found for $r_{e,1.6}$. These intercollection $r_e$ differences result in relatively larger estimates of C6 CDNC for both channels. Nevertheless, CDNC from these two spectral channels offer similar annual cycles for both C5.1 and C6, regardless of the geographic region. $N_{3.7}$ differences are more subtle and, unlike $N_{1.6}$ and $N_{2.1}$, rarely is the sign of the differences temporally uniform. Moreover, the global intercollection differences in $r_{e,3.7}$ and $N_{3.7}$ exhibit quite different behavior than those derived from the 1.6 and 2.1μm channels. These differences are inherently attributable to the more

25   wholesale C6 changes that addressed known shortcomings in the C5.1 $r_{e,3.7}$ retrieval, but because the individual effects of the

C6 changes can be quite large, are often of opposite sign, and have angular and potentially other unknown dependencies, it remains unclear how granule-level $r_{e,3.7}$ differences translate to the global aggregated differences shown here. It is therefore ill-advised to draw conclusions from the $r_{e,3.7}$ and $N_{3.7}$ intercollection differences and, furthermore, it is recommended that quantitative uses of the C5.1 $r_{e,3.7}$ retrieval be avoided given its known shortcomings.

5        Among the updates for C6 is the independent reporting of $r_e$ for each wavelength, rather than as differences with respect to $r_{e,2.1}$, as well as the inclusion of retrievals of the so-called partly cloudy pixels previously discarded in C5.1. These changes offer additional options in the analysis of CDNC from MODIS. Several permutations in data screening scenarios beyond those used in this study are now available which were not possible in C5.1, and will be explored in future studies. Caution will be warranted, however, when interpreting the results of these and other future studies of $r_e$ and CDNC inter-

10    comparisons of different pixel populations given the differences observed here for overcast scenes only between spectrally independent and common pixels.

**References**

Ahmad, I., Mielonen, T., Grosvenor, D. P., Portin, H. J., Arola, A., Mikkonen, S., Kuhn, T., Leskinen, A., Joutsensaari, J.,
15    Komppula, M., Lehtinen, K. E. J., Laaksonen, A., and Romakkaniemi, S.: Long-term measurements of cloud droplet concentrations and aerosol-cloud interactions in continental boundary layer clouds, Tellus B, 65, ARTN 20138 10.3402/tellusb.v65i0.20138, 2013.

Albrecht, B. A.: Aerosols, Cloud Microphysics, and Fractional Cloudiness, Science, 245, 1227-1230, 1989.

Baum, B. A., Menzel, W. P., Frey, R. A., Tobin, D. C., Holz, R. E., Ackerman, S. A., Heidinger, A. K., and Yang, P.:
20    MODIS Cloud-Top Property Refinements for Collection 6, J Appl Meteorol Clim, 51, 1145-1163, 2012.

Bennartz, R.: Global assessment of marine boundary layer cloud droplet number concentration from satellite, J Geophys Res-Atmos, 112, Artn D02201
Doi 10.1029/2006jd007547, 2007.

Bennartz, R., Fan, J. W., Rausch, J., Leung, L. R., and Heidinger, A. K.: Pollution from China increases cloud droplet
25    number, suppresses rain over the East China Sea, Geophys Res Lett, 38, 2011.

Brenguier, J. L., Pawlowska, H., Schuller, L., Preusker, R., Fischer, J., and Fouquart, Y.: Radiative properties of boundary layer clouds: Droplet effective radius versus number concentration, J Atmos Sci, 57, 803-821, 2000.

Brenguier, J. L., Burnet, F., and Geoffroy, O.: Cloud optical thickness and liquid water path - does the k coefficient vary with droplet concentration?, Atmos Chem Phys, 11, 9771-9786, Doi 10.5194/Acp-11-9771-2011, 2011.

5   Brioude, J., Cooper, O. R., Feingold, G., Trainer, M., Freitas, S. R., Kowal, D., Ayers, J. K., Prins, E., Minnis, P., McKeen, S. A., Frost, G. J., and Hsie, E. Y.: Effect of biomass burning on marine stratocumulus clouds off the California coast, Atmos Chem Phys, 9, 8841-8856, 2009.

Cho, H. M., Zhang, Z. B., Meyer, K., Lebsock, M., Platnick, S., Ackerman, A. S., Di Girolamo, L., C-Labonnote, L., Cornet, C., Riedi, J., and Holz, R. E.: Frequency and causes of failed MODIS cloud property retrievals for liquid phase clouds over
10  global oceans, J Geophys Res-Atmos, 120, 4132-4154, 10.1002/2015jd023161, 2015.

Cox, C., and Munk, W.: Statistics of the sea surface derived from Sun glitter, Journal of Marine Research, 13, 198-227, 1954a.

Cox, C., and Munk, W.: Measurement of the Roughness of the Sea Surface from Photographs of the Sun's Glitter, J. Opt. Soc. Am., 44, 838-850, 10.1364/JOSA.44.000838, 1954b.

15  Duynkerke, P. G., de Roode, S. R., van Zanten, M. C., Calvo, J., Cuxart, J., Cheinet, S., Chlond, A., Grenier, H., Jonker, P. J., Kohler, M., Lenderink, G., Lewellen, D., Lappen, C. L., Lock, A. P., Moeng, C. H., Muller, F., Olmeda, D., Piriou, J. M., Sanchez, E., and Sednev, I.: Observations and numerical simulations of the diurnal cycle of the EUROCS stratocumulus case, Q J Roy Meteor Soc, 130, 3269-3296, Doi 10.1256/Qj.03.139, 2004.

Ho, S. P., Peng, L., Anthes, R. A., Kuo, Y. H., and Lin, H. C.: Marine Boundary Layer Heights and Their Longitudinal,
20  Diurnal, and Interseasonal Variability in the Southeastern Pacific Using COSMIC, CALIOP, and Radiosonde Data, J Climate, 28, 2856-2872, 10.1175/Jcli-D-14-00238.1, 2015.

Huneeus, N., Gallardo, L., and Rutllant, J. A.: Offshore transport episodes of anthropogenic sulfur in northern Chile: Potential impact on the stratocumulus cloud deck, Geophys Res Lett, 33, 10.1029/2006gl026921, 2006.

Lohmann, U., and Feichter, J.: Global indirect aerosol effects: a review, Atmos Chem Phys, 5, 715-737, 2005.

25  Marchant, B., Platnick, S., Meyer, K., Arnold, G. T., and Riedi, J.: MODIS Collection 6 shortwave-derived cloud phase classification algorithm and comparisons with CALIOP, Atmos Meas Tech, 9, 1587-1599, 10.5194/amt-9-1587-2016, 2016.

Martin, G. M., Johnson, D. W., and Spice, A.: The Measurement and Parameterization of Effective Radius of Droplets in Warm Stratocumulus Clouds, J Atmos Sci, 51, 1823-1842, 1994.

Menzel, W. P., Frey, R. A., Zhang, H., Wylie, D. P., Moeller, C. C., Holz, R. E., Maddux, B., Baum, B. A., Strabala, K. I., and Gumley, L. E.: MODIS global cloud-top pressure and amount estimation: Algorithm description and results, J Appl
5   Meteorol Clim, 47, 1175-1198, 10.1175/2007jamc1705.1, 2008.

Nakajima, T., and King, M. D.: Determination of the Optical-Thickness and Effective Particle Radius of Clouds from Reflected Solar-Radiation Measurements .1. Theory, J Atmos Sci, 47, 1878-1893, 1990.

Painemal, D., and Zuidema, P.: Assessment of MODIS cloud effective radius and optical thickness retrievals over the Southeast Pacific with VOCALS-REx in situ measurements, J Geophys Res-Atmos, 116, Artn D24206
10   10.1029/2011jd016155, 2011.

Pawlowska, H., and Brenguier, J. L.: An observational study of drizzle formation in stratocumulus clouds for general circulation model (GCM) parameterizations, J Geophys Res-Atmos, 108, 10.1029/2002jd002679, 2003.

Platnick, S.: Vertical photon transport in cloud remote sensing problems, J Geophys Res-Atmos, 105, 22919-22935, 2000.

Platnick, S., King, M. D., Meyer, K. G., Wind, G., Amarasinghe, N., Marchant, B., Arnold, G. T., Zhang, Z., Hubanks, P. A.,
15   Ridgway, W., and Riedi, J.: MODIS Cloud Optical Properties: User Guide for the Collection 6 Level-2 MOD06/MYD06 Product and Associated Level-3 Datasets, 2015.

Platnick, S., Meyer, K. G., D., K. M., Wind, G., Amarasinghe, N., Marchant, B., Arnold, G. T., Zhang, Z., Hubanks, P. A., Holz, R. E., Yang, P., Ridgway, W. L., and Riedi, J.: The MODIS cloud optical and microphysical products: Collection 6 updates and examples from Terra and Aqua, Geoscience and Remote Sensing, IEEE Transactions on, in revision, 2016.

20   Roberts, G., Wooster, M. J., and Lagoudakis, E.: Annual and diurnal african biomass burning temporal dynamics, Biogeosciences, 6, 849-866, 2009.

Twomey, S.: Pollution and Planetary Albedo, Atmos Environ, 8, 1251-1256, 1974.

von Engeln, A., and Teixeira, J.: A Planetary Boundary Layer Height Climatology Derived from ECMWF Reanalysis Data, J Climate, 26, 6575-6590, 10.1175/Jcli-D-12-00385.1, 2013.

25   Zeng, S., Riedi, J., Trepte, C. R., Winker, D. M., and Hu, Y. X.: Study of global cloud droplet number concentration with A-Train satellites, Atmos Chem Phys, 14, 7125-7134, 10.5194/acp-14-7125-2014, 2014.

Zhang, Z. B., and Platnick, S.: An assessment of differences between cloud effective particle radius retrievals for marine water clouds from three MODIS spectral bands, J Geophys Res-Atmos, 116, 2011.
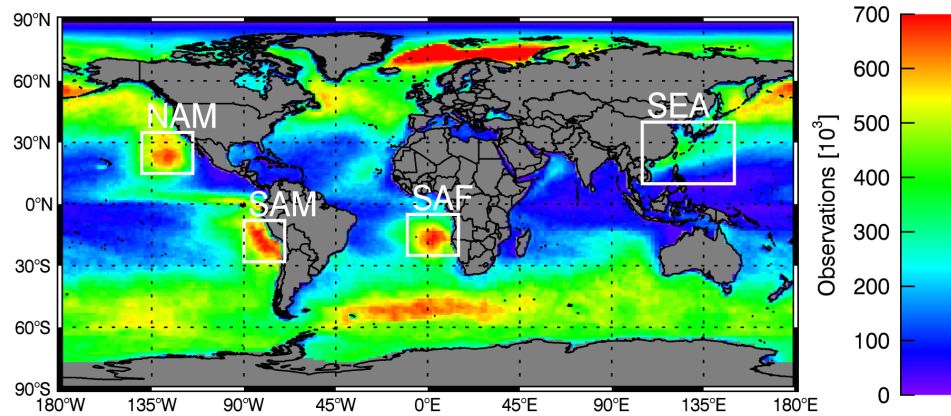
**Figure 1: Annual total of MODIS Aqua common pixel observations per 1 x 1 degree grid box. Focus regions are overlain.**
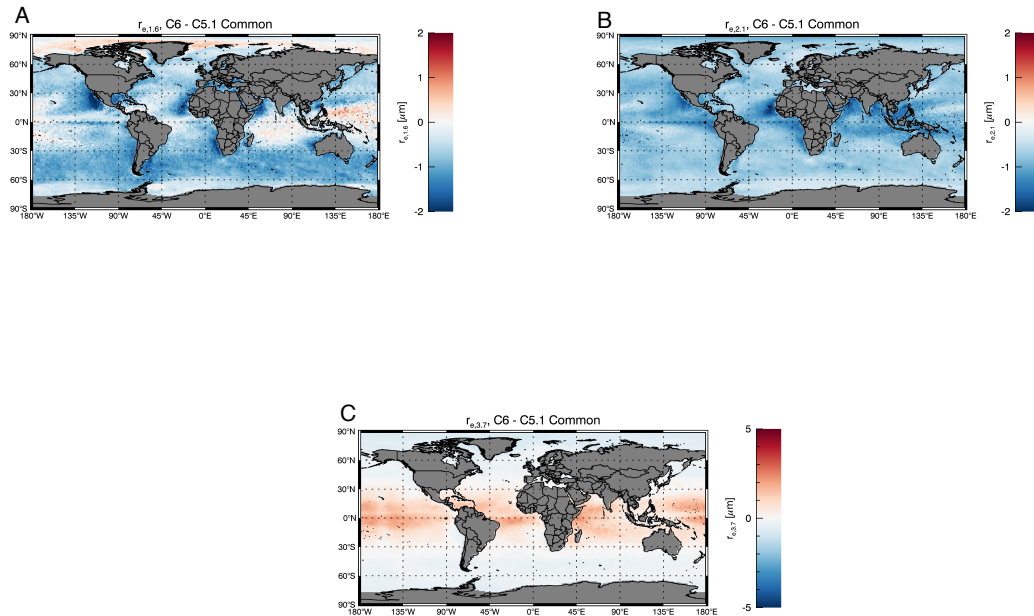
Figure 2: Difference between mean annual C6 – C5.1 effective radius for calendar year 2008 for pixels common to both cloud products for a) 1.6 μm, b) 2.1 μm and c) 3.7 μm.
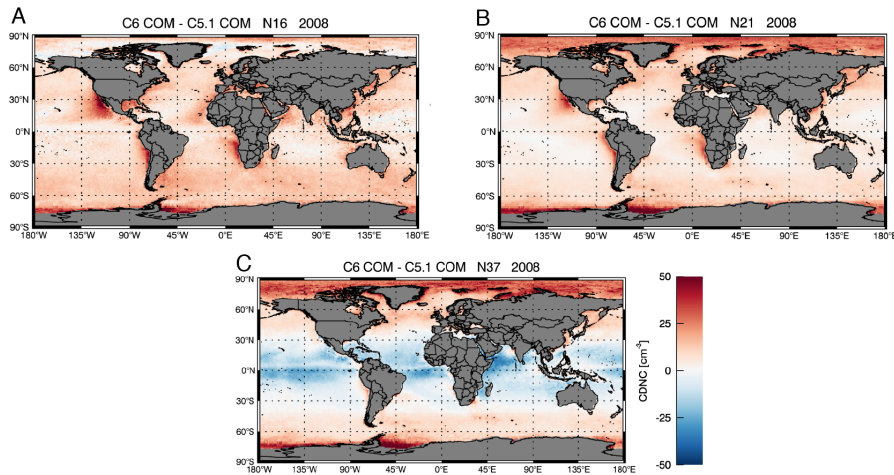
**Figure 3: Difference between mean annual C6 – C5.1 CDNC for calendar year 2008 for pixels common to both cloud products for**

**a) 1.6 μm, b) 2.1 μm and c) 3.7 μm.**
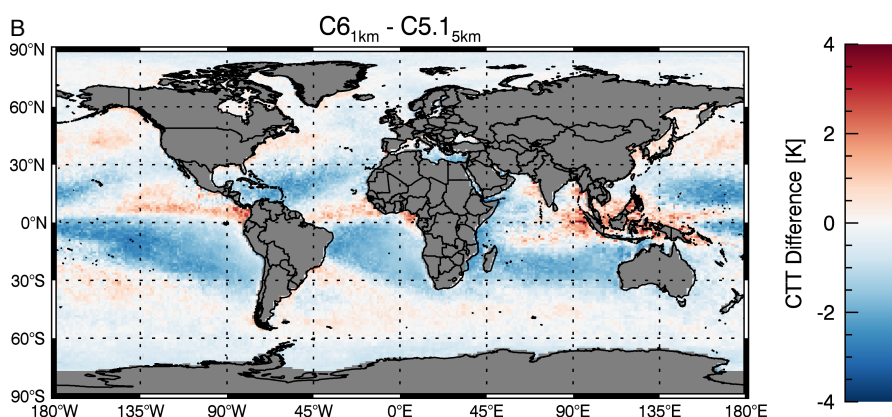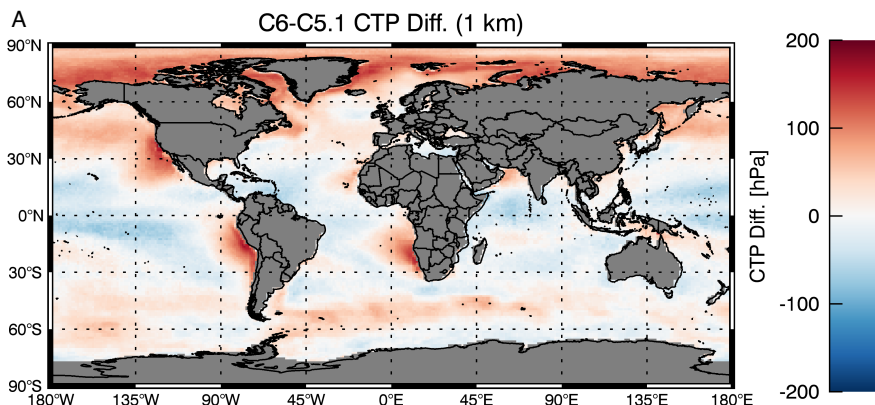
**Figure 4: Cloud top pressure (a) and temperature (b) differences between aggregated 1 km resolution C6 and 5 km resolution C5.1 for the common pixel population.**
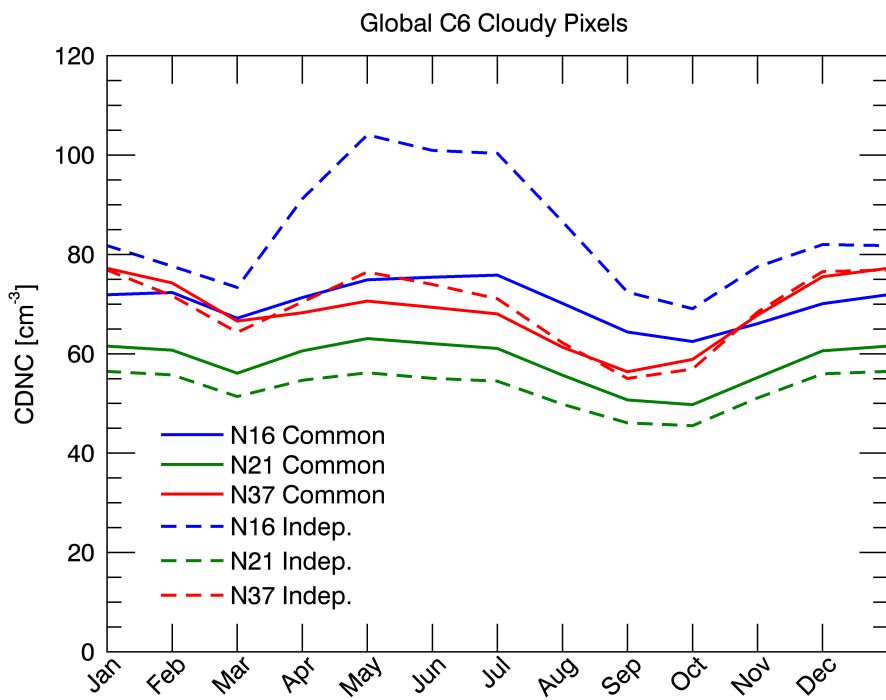
**Figure 5: Global average CDNC retrievals for pixels with valid $r_e$ retrievals for all three channels (Common) and pixels with one or more value retrieval (Independent).**
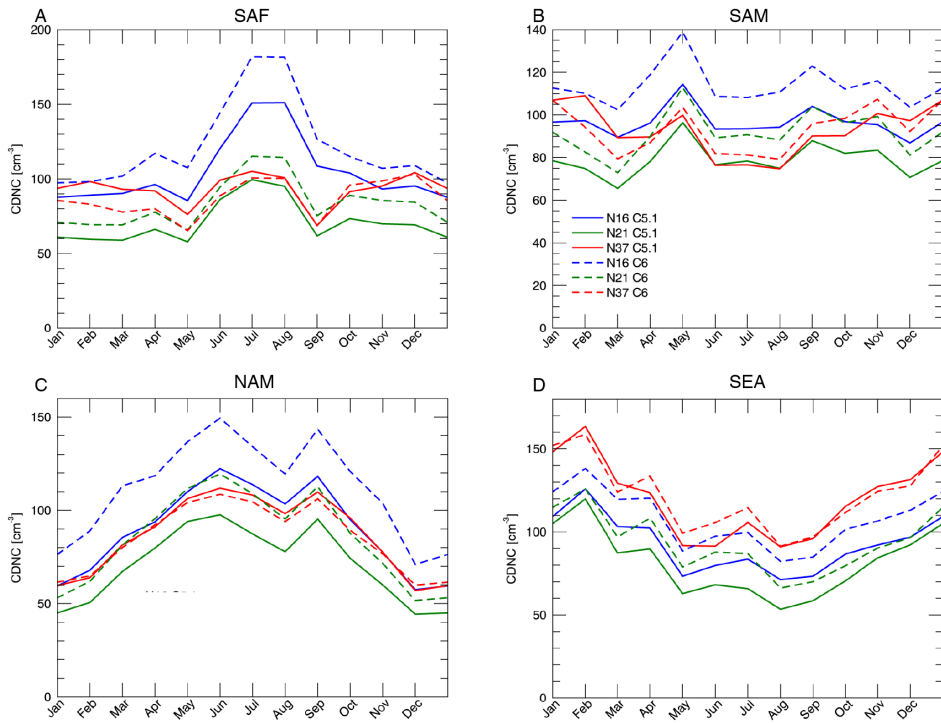
**Figure 6: Annual CDNC cycle plots for the a) Southern African, b) South American, c) North American and d) Southeast Asian regions.**